Lasers in Manufacturing Conference 2025

Investigation of a melt pool temperature control for the additive manufacturing process of tool components using laser directed energy deposition

Eike Tim Koopmann[1,*], Leonard Simon Plutz[1], Leonard Schmitz[1], Christoph Kaminsky[1], Henning Zeidler[2]

[1]*Mercedes-Benz AG, Sindelfingen, Germany*
[2]*Institute for Machine Elements, Design and Manufacturing, TU Bergakademie Freiberg, Freiberg, Germany*

Abstract

In the automotive industry, the increasing number of product variants requires a high degree of flexibility, offering new applications for additive manufacturing processes. A promising and cost-effective approach is the hybrid additive manufacturing of tool components using directed energy deposition (DED). A key factor in the process is the laser power, as the temperature gradient between substrate and additive build-up has a significant influence on the formation of cracks and the contour accuracy of the component. In this paper, a laser power control system is investigated with the aim of keeping the melt pool temperature constant to reduce geometric deviations and residual stresses resulting from excessive heat input into the component. For this purpose, welding specimens are manufactured additively, followed by an optical measurement and a metallographic analysis to identify part defects. The results are used to produce a tool component with an optimized hybrid additive manufacturing strategy.

Keywords: Additive manufacturing; directed energy deposition; tool components; pyrometry, temperature control

1. Introduction

In the highly competitive automotive industry, additive manufacturing (AM) delivers a significant advantage by enabling the economic and flexible production of complex tool components (Vasco, 2021). Combining AM with conventional subtractive manufacturing methods, also known as hybrid additive manufacturing, overcomes the limitations of AM by ensuring a cost-efficient production process. Furthermore, the near net shape production of AM parts minimizes the machining time while the subtractive process enables high-quality surface finishes and precise geometric dimensions (Pragana et al., 2021; Dass and Moridi, 2019). In this context, directed energy deposition (DED) and powder bed fusion (PBF) are established as the leading technologies in metal additive manufacturing (Salunkhe and Rajamani, 2023). PBF is mainly used for complex structures with cooling channels and overhang features due to the high resolution of the process and the unused powder providing integrated support (Babuska et al., 2021). While PBF is generally limited to a single material for each part, DED allows the implementation of graded structures and a multi-material build-up, providing a functional design of tool components optimised for the respective stress conditions (Ansari, Jabari and Toyserkani, 2021; Feenstra et al., 2021). DED is also characterized by high deposition rates with a coarser resolution making it ideal for the manufacturing of large components (Kumar et al.,2016) and the repair of tool components due to its feasibility of application on existing structures. Additionally, the grain structure of the material can be modified for the specific application by optimizing the process parameters (Tofail et al., 2018; Chechik et al., 2023).

In this context, the use of tool steel in the DED process represents a major challenge due to its high carbon content and limited weldability (Belitz, Scheider and Zeidler, 2021). Especially for multi-layer parts, the residual stresses increase with

* Corresponding Author. Tel.: +49 160 8623667. Email address: eike_tim.koopmann@mercedes-benz.com

the build height due to the higher number of thermal heating cycles and the thermal load (Jing et al., 2022). This leads to the formation of cracks in the part and, in case of a tool component, to an exclusion for the application in series production (Gao et al., 2013). To overcome this manufacturing limitation, a part-dependent and optimized welding strategy with adjusted process parameters is essential (Koopmann, Jäger and Zeidler, 2025).

Numerous studies focussed on analysing the heat distribution for different geometries by measuring the melt pool size or temperature at a constant laser power. Urresti et al. used a pyrometer to monitor the heat accumulation across a single welding track in the DED process. The investigations with laser powers from 540 to 660 W showed a constant melt pool temperature and melt pool size for each single track (Urresti et al., 2024). In case of a multi-track buildup, Farshidianfar et al. analysed the melt pool temperature with an infrared camera for thin walls consisting of five vertical tracks. At a laser power of 800 W, an almost constant melt pool temperature of 1500 °C was measured for the first track, while for the fifth track the temperature in the welding process increased up to 2000 °C due to heat accumulation (Farshidianfar et al., 2021). Maffia et al. investigated a similar result for the melt pool temperature profile of thin-walled tubes by using a pyrometer and laser power of 500 W. Measuring a temperature of 1650 °C in the first track, the melt pool temperature increased during the process and reached 1900 °C in the eightieth track. Furthermore, Maffia et al. demonstrated the impact of the geometry for thin-walled tubes. Compared to a tube diameter of 24 mm, a smaller diameter of 14 mm showed a 100 °C higher melt pool temperature due to reduced heat dissipation (Maffia, Valentina and Barbara, 2023). For the manufacturing of multi-layer geometries, Azab et al. showed the effect of heat accumulation by analysing the melt pool temperature profile of a cube with 35 layers. In the first 25 layers, a temperature increase of 1700 °C to 1830 °C and a doubling of the melt pool size due to the large welding mass were measured by the thermal camera at a laser power of 390 W (El-Azab et al., 2023).

A promising approach to avoid overheating in the geometry and to minimize the effort of extensive parameter studies is the implementation of a combined process monitoring and laser power control system, as it measures either the melt pool size or temperature and adjusts the laser power for equal thermal conditions in the DED process independent from the part geometry (Ocylok et al., 2014; Ali et al., 2022). Besides this, there are also approaches for controlling e.g. the powder mass flow, whereby the response time requires several seconds for a constant mass flow, in contrast to microseconds for the laser power, so that real-time control is not feasible (Song et al., 2012). In the literature, closed-loop controls of laser power have already been implemented in the DED process for the manufacturing of basic geometries such as single tracks, thin walls or cylinders and small blocks (Bernauer et al., 2022; Akbari and Kovacevic, 2019; Smoqi et al., 2022; Freeman et al., 2023; Song et al., 2012). Bernauer et. al designed a pyrometer based closed-loop process control for DED, keeping the melt pool at a constant temperature. Validation experiments of single tracks using stainless steel 316L on AISI 304 substrates with varying thickness showed that the melt pool temperature was maintained at the reference temperature by adjusting the laser power and additionally demonstrated the robustness of the process control for rapidly changing process conditions (Bernauer et al., 2022). Akbari and Kovacevic used the melt pool width as monitored and the laser power as controlled parameter for a closed-loop control of the DED process. With this set-up, they welded thin walls consisting of 160 single tracks on AISI 304L stainless steel substrates by utilizing 316L powder material. The results have shown a constant single track width and a higher geometric accuracy compared to the experiments with constant laser power, in which an increased melt pool and track width was determined with an increasing number of layers (Akbari and Kovacevic, 2019). Smoqi et al. applied a pyrometer based closed-loop control for DED and 316L powder on stainless steel substrates, demonstrating the usability of the control system by manufacturing thin trapezoid-shaped parts consisting of four overlapping tracks in a layer and 198 layers in total with a set melt pool temperature and varying laser power. The closed-loop control mitigated heterogeneity in the microstructure and reduced deviations in porosity and microhardness compared to parts produced with constant parameters (Smoqi et al., 2022). Freeman et. al developed a camera-based image processing control measuring the melt pool width with a coaxial camera for the adjustment of the laser power. They verified the system by manufacturing 316L square steel blocks with a base area of 13.6 mm x 50 mm and up to 55 layers but faced issues such as geometry dependent heat loss mechanisms and noisy data as the laser changed direction in the build-up process (Freeman et al., 2023). Song et al. designed a two-input-single-output controller for a DED process, monitoring the melt pool temperature with a pyrometer and the melt pool height with three high speed cameras to keep the melt pool temperature and height constant by adjusting the laser power. Furthermore, they fabricated a complex turbine blade with 316L stainless steel powder, avoiding over- and under-building through an optimized heat input and layer height (Song et al., 2012).

In this work, the material 3.33 LOWC is additively deposited on the cold work tool steel 1.2333 by using a DED process in combination with a pyrometer-based closed-loop control. Furthermore, the aim is an optimization of the laser power input to increase the geometric accuracy as well as to reduce the thermal load in the additive build-up of a large tool component. As a first step, the influence of spot diameter, powder mass flow, feed rate and laser power on the melt pool temperature are investigated for single tracks. Based on these results, a cube geometry with constant and controlled laser power is welded to compare the geometric accuracy. Finally, the closed-loop control of the laser power is utilized for the additive manufacturing of a complex shear cutting tool.

2. Experimental procedure

2.1 Material

The cold work steel G59CrMoV18-5 (1.2333) from Dörrenberg Edelstahl with a carbon content of 0.6 %, a chromium content of 4.5 % and a manganese content of 0.8 % is used as substrate material for all experiments. Because of its good weldability and surface hardenability, the steel is conventionally utilized for the production of deep-drawing and cutting tools. For the additive build-up, 3.33 LOWC from Höganäs AB with a particle size range from 45 to 150 µm is used as feedstock material. Based on a carbon content of 0.2 % and a chromium content of 28 %, the material offers a high toughness and ductility, which is a main requirement for the repair and modification of tool geometries. An overview of the chemical composition of 1.2333 and 3.33 LOWC is shown in Table 1.

Table 1. Chemical composition of substrate material and powder feedstock in weight percent (wt.-%)

Elements (wt.-%)	Fe	C	Cr	Ni	Mo	Mn	Si	V
1.2333	Bal.	0.6	4.5	-	0.5	0.8	0.4	0.2
3.33	Bal.	0.2	28	16	4.5	0.65	1.2	-

2.2 Experimental set-up

For the experiments in this work, a multifunctional system HARD+CLAD from ERLAS (Erlanger Lasertechnik GmbH) is used, offering laser beam welding and hardening in a single system. In addition, a Laserline diode laser, type LDF 4000-40, with a maximum laser power of 4000 W and a wavelength between 900 - 1100 nm is utilized as laser source. The optical parameters in the laser processing optic are kept constant with a focal laser diameter of 3.5 mm, a focal length of 350 mm and a collimation length of 105 mm. Moreover, a 3-jet-powder-nozzle from Fraunhofer ILT is attached to the processing optic and the 6-axis robotic system KUKA KR480 R3330, whereby a working distance of 12 mm is selected between nozzle and substrate. Furthermore, a PF 4/4 powder feeder unit from the manufacturer GTV Verschleißschutz GmbH ensures a constant powder mass flow for all experiments. To protect the melt pool and realize the powder mass flow, Argon is used as shielding and carrier gas with a volume flow rate of 6 liters per minute each. For the measurement of the melt pool temperature, the two-color pyrometer Metis M322 from SensorTherm GmbH is coaxially integrated into the beam path of the laser by utilizing a dichroic mirror. In this context, the pyrometer has a measuring range from 600 °C to 2.300 °C with a spectral range of 1.65 µm-1.8 µm for the first and 1.45 µm-1.65 µm for the second channel.

2.3 Methodology

The aim of this work is to develop a melt pool temperature control for the additive manufacturing of complex tool components. For this reason, individual tracks with a length of 100 mm are welded on a substrate with dimensions of 115 x 45 x 30 mm to analyse the influence of different process parameters on the melt pool temperature. The initial parameters in the experiments are a laser power of 1600 W, a pyrometer spot diameter of 3.5 mm, a scan speed of 19 mm/s and a powder mass flow of 17.9 g/min. Based on these parameters, the spot diameter of the pyrometer is increased to 5.5 mm and 7.5 mm with the aim of analysing the influence on the measured melt pool temperature. As a second influential parameter, the powder mass flow is systematically varied in a range of 0.5 to 31.7 g/min, while all further parameters correspond to the initial configuration. To investigate the influence of the scan speed on the melt pool temperature, different scan speeds of 10, 15, 19 and 25 mm/s are used in further experiments. Finally, the laser power is varied in a range from 1200 W to 2520 W in order to determine the temperature monitoring limits of the pyrometer. For all experiments, a metallographic analysis is carried out, which includes water jet cutting, cut-off grinding and warm embedding. To prepare the specimens for optical analysis, different polishing processes using diamond suspensions with grain sizes of 9, 3, and 1 µm are conducted. The geometric characterization of the single tracks as well as the identification of defects is performed utilizing a Leica DMRM optical microscope and the software Olympus Stream Enterprise.

In the second step, a single layer with a base area of 55 by 55 mm is welded using the initial parameters to analyse the heat distribution within a multi-track geometry and define the target temperature for the melt pool temperature control. The experiments are carried out with a single track width of 3.2 mm and a track offset of 1.6 mm, resulting in an overlap ratio of 50 %.

A cube with a base area of 55 x 55 mm and 63 layers is used as a comparative geometry for the open-loop and closed-

loop controlled welding process. Based on the initial parameters, a meandering infill strategy is selected within a layer. Additionally, an outer contour with a constant laser power of 1200 W is welded at the start of each layer with the aim of ensuring the geometric accuracy in the additive build-up. To further avoid directional dependencies and overbuilding in the process, the welding start point as well as the orientation of the single tracks are rotated by 90 degrees around the z-axis in each layer. The first three layers are welded with a constant laser power of 2200 W to increase the bonding quality between the substrate 1.2333 and 3.33 LOWC. In the uncontrolled process, the additive build-up is manufactured with a constant laser power of 1600 W and a z-offset of 0.55 mm. For the closed-loop controlled process, a target melt pool temperature of 2200 °C and a z-offset of 0.45 mm are used to manufacture the cube. Furthermore, the closed-loop control is designed as a PI controller with a proportional gain of 0.035 and an integration time of 30 ms, whereby the integration time at the start of the welding process is set to 10 % of the initial time due to process instabilities. In order to maintain a minimum laser power of 800 W for stable process conditions, a waiting time of 600 seconds is implemented after every 12 layers, which is also applied in the open-loop process. The deviation of the welded geometry from the CAD model is measured using the Atos III system from GOM Metrology and the ATOS Professional 2018 software. Furthermore, a hardness measurement is carried out to analyse the influence of the laser power reduction in the closed-loop controlled process. For this purpose, samples of both cube geometries are prepared metallographically and etched with a V2A solution to visualize grain boundaries and single welding tracks. Subsequently, the HV 1 hardness is evaluated using five measuring points in layers 2, 7, 12 to check the required minimum hardness of 300 HV.

The validation results of the closed-loop control are utilized to additively manufacture a complex punch. As part of a cutting segment in a metal forming tool, the punch is used for shearing off excess material and thereby achieving the final geometry of the sheet metal outer skin part. While all process parameters are adopted from the previous experiments, the base area is enlarged to 60 by 65 mm for the punch geometry. The entire punch consists of 75 layers, divided into 21 layers for the base body and 54 layers for the complex upper part of the punch. To demonstrate a repair case of a tool component, in which the worn punch is milled down to the base body, only the complex upper part is welded onto the substrate. In a second experiment, the entire punch is produced in order to investigate the usability of the closed-loop control system for larger tool components.

3. Results and discussion

A decisive factor in AM processes is the geometric accuracy and a defect-free additive build-up of the part. Especially in the DED process, the optimal energy input is a major challenge, as excessive laser power can lead to an overheating of the additive build-up, resulting in local geometric deviations and process instabilities. For this reason, the monitoring of the melt pool temperature process must be highly precise to achieve an optimal energy input with the closed-loop control. Figure 1 shows the melt pool temperature for the pyrometer spot diameters of 3.5 mm, 4.5 mm and 7.5 mm. Additionally, Figure 1 demonstrates that the melt pool temperature is monitored for all spot diameters in the relevant laser power range of 1600 W to 2520 W, as the maximum pyrometer temperature of 2300 °C is not reached in any case. In general, the melt pool temperature increases almost linearly with the laser power. As the pyrometer spot diameters of 4.5 mm and 7.5 mm exceed the laser focus diameter of 3.5 mm, cold areas outside the melt pool are measured. This leads, exemplary for a laser power of 1600 W, to a lower melt pool temperature of 1740 °C and 1577 °C instead of 2004 °C for a pyrometer spot of 3.5 mm. Moreover, the increasing ratio of cold areas is also the reason for a lower linear increase in melt pool temperature at higher laser powers for both larger spot diameters. For this reason, a spot diameter of 3.5 mm is used for further experiments to ensure a precise measurement of the melt pool temperature.

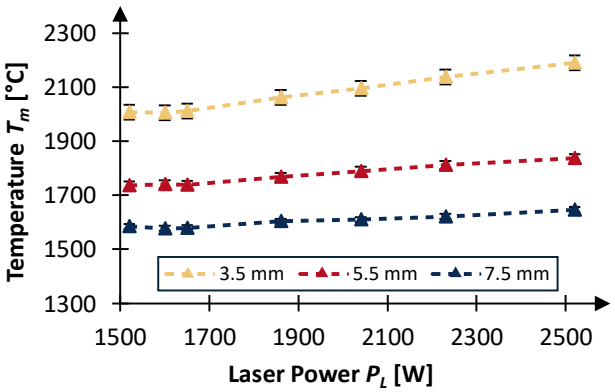

Figure 1. Influence of the laser power on the melt pool temperature T_m for single tracks and laser spot diameters of 3.5 mm, 5.5 mm and 7.5 mm

The melt pool temperature is also influenced by the powder mass flow in the welding process. In this context, Figure 2 a) shows the melt pool temperature profile for a single track and different powder mass flow rates, where a constant temperature with small deviations is visible for each track. Moreover, the melt pool temperature decreases linearly with increasing powder mass flow (Figure 2 b), as the additional powder in the process has a cooling effect on the melt pool. In total, melt pool temperatures in the range of 1913 °C to 2148 °C are measured for the powder mass flow rates of 0.5 g/min to 31.7 g/min.

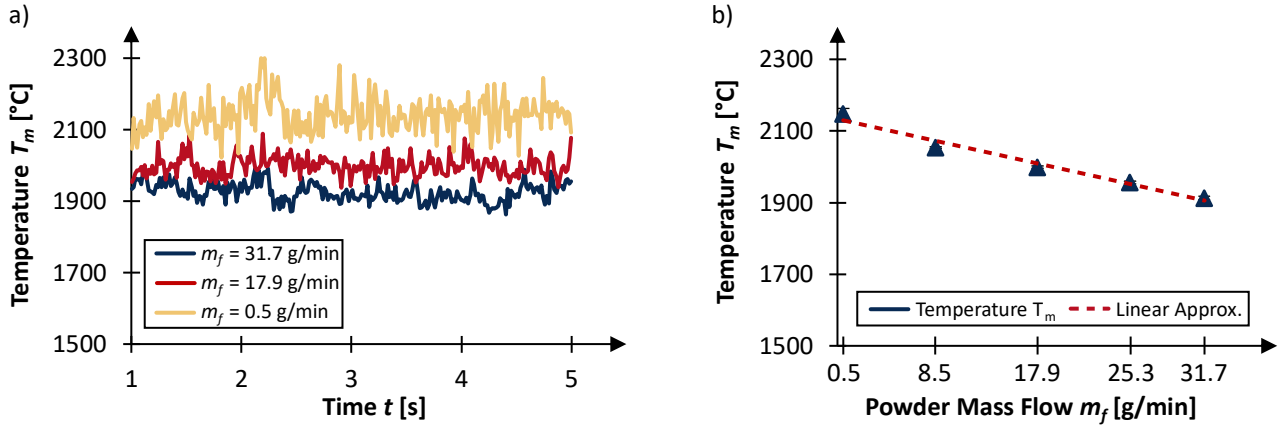

Figure 2. Influence of the powder mass flow on the melt pool temperature T_m for single tracks (a) Time-temperature data of the homogeneous phase ($1\,s \leq t \leq 5\,s$) and (b) approximated linear relation between powder mass flow and resulting melt pool temperature T_m

The results of the metallographic analysis are visualized in Figure 3 a). While the track width remains almost constant, the single track height increases by up to 0.25 mm due to the increased powder mass flow rate. Simultaneously, the meltdown depth decreases from 0.49 mm to 0.26 mm, as the energy is used to melt the powder and less energy is absorbed by the substrate. Especially for a powder mass flow of 8.5 g/min in Figure 3 b), a vertical crack appears in the single track, caused by residual stresses and the high melt pool depth. In contrast, all higher powder mass flow rates show a uniform track build-up similar to Figure 3 c).

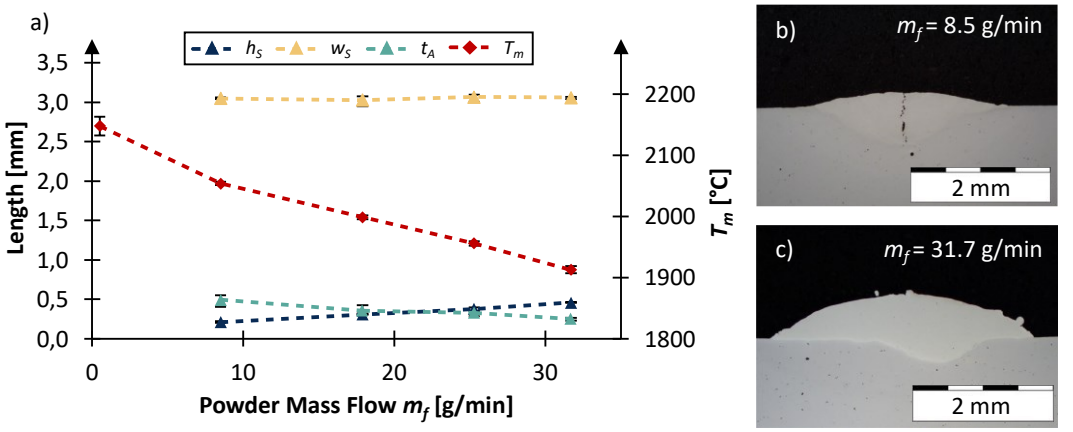

Figure 3. (a) Metallographic analysis of the parameters track height h_S, track width w_S, melt pool depth t_A and melt pool temperature T_m for different powder mass flows m_f; (b) cross-section of a single track with a powder mass flow of m_f = 8.5 g/min and (c) m_f = 31.7 g/min

Furthermore, the influence of the scan speed on the melt pool temperature is shown in Figure 4 a) and b). While the melt pool temperature profile within a single track is nearly constant for the varying scan speeds, excluding start and stop phases due to inconsistent process conditions, a similar average temperature between 1993 °C and 2002 °C is measured for the three lowest scan speeds. In this context, the scan speed of 25 mm/s is an exception with a melt pool temperature of 1913 °C.

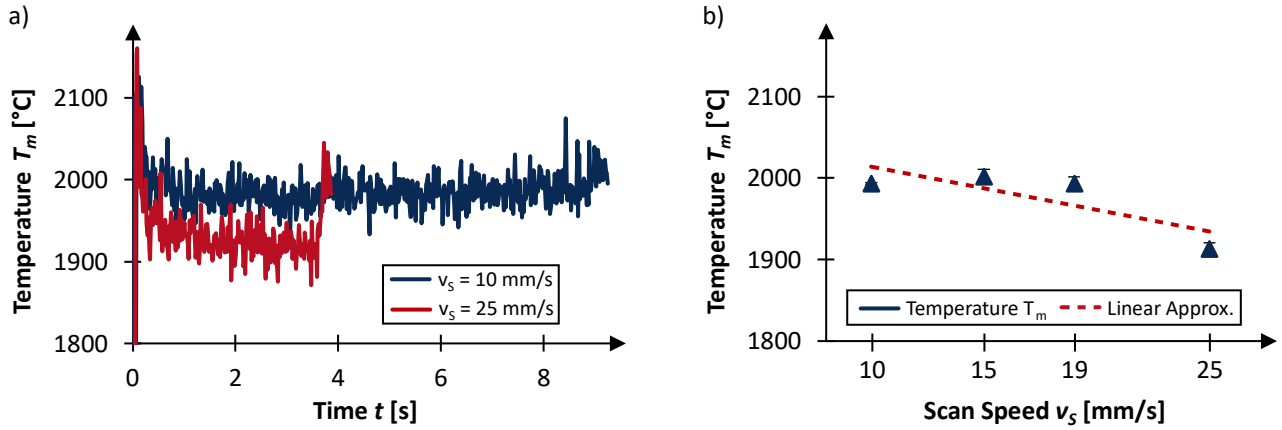

Figure 4. Influence of the scan speed v_S on the melt pool temperature T_m for single tracks (a) Time-temperature data and (b) approximated linear relation between scan speed v_S and resulting melt pool temperature T_m

As visualized in Figure 5 a), the lower energy input per area reduces the melt pool depth in the substrate from 0.73 mm to 0.47 mm as well as the height of the single track from 0.73 mm to 0.27 mm. In addition, the cross sections from the metallographic analysis in Figure 5 b) and c) demonstrate exemplarily, that a defect-free single track with a homogeneous grain structure is welded for all scan speeds in the range of 10-25 mm/s.

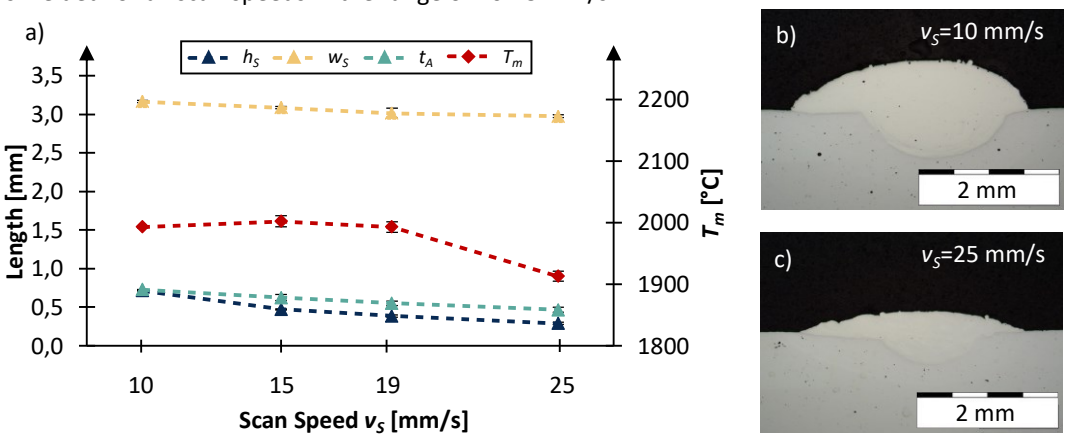

Figure 5. (a) Metallographic analysis of the parameters track height h_S, track width w_S, melt pool depth t_A and melt pool temperature T_m for different scan speeds v_S; (b) cross-section of a single track with a scan speed of v_S = 10 mm/s and (c) v_S = 25 mm/s

Finally, the influence of the laser power on the melt pool temperature is investigated in more detail. Compared to the single track experiments with a varying powder mass flow or scan speed, the melt pool temperature profiles for the different laser powers in Figure 6 a) show the smallest deviations within a track. Moreover, the laser power shows an almost linear

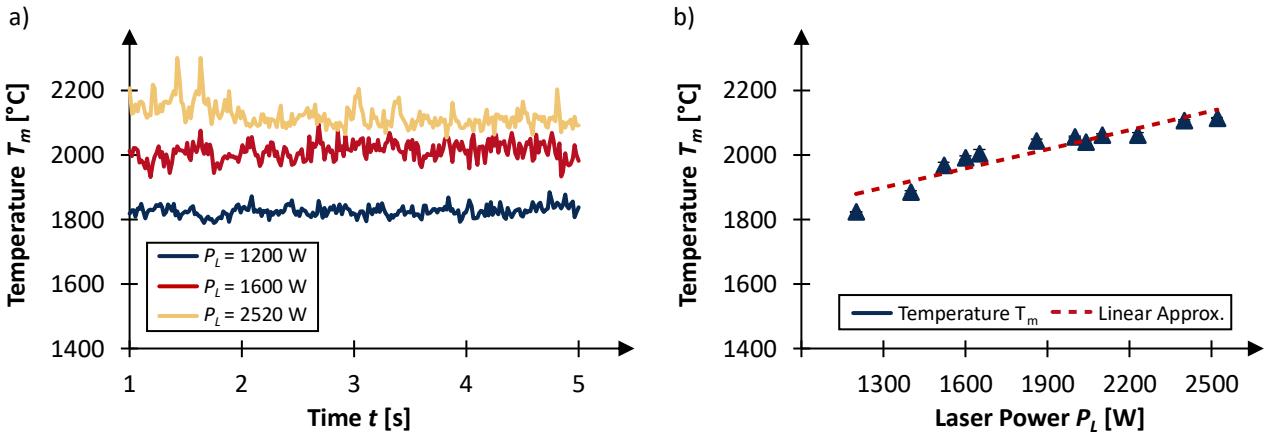

Figure 6. Influence of the laser power P_L on the melt pool temperature T_m for single tracks (a) Time-temperature data and (b) approximated linear relation between laser power P_L and resulting melt pool temperature T_m

correlation with the melt pool temperature. At the lowest laser power of 1200 W, a melt pool temperature of 1824 °C is recorded, whereby a maximum temperature of 2114 °C is measured for a laser power of 2520 W.

The metallographic analysis in Figure 7 a) shows the increasing meltdown depth from 0.3 mm to 0.9 mm as well as the increasing track width from 2.88 mm to 3.18 mm for a laser power of 2520 W. For the track height, an increase from 0.3 mm to 0.44 mm is observed in the range of 1200 to 2520 W. The Gaussian laser profile leads to an uneven energy distribution across the entire laser focus diameter, further resulting in an excessive energy input in the center of the track and vertical crack formation for the highest laser power of 2520 W, as demonstrated in Figure 7 b) and c).

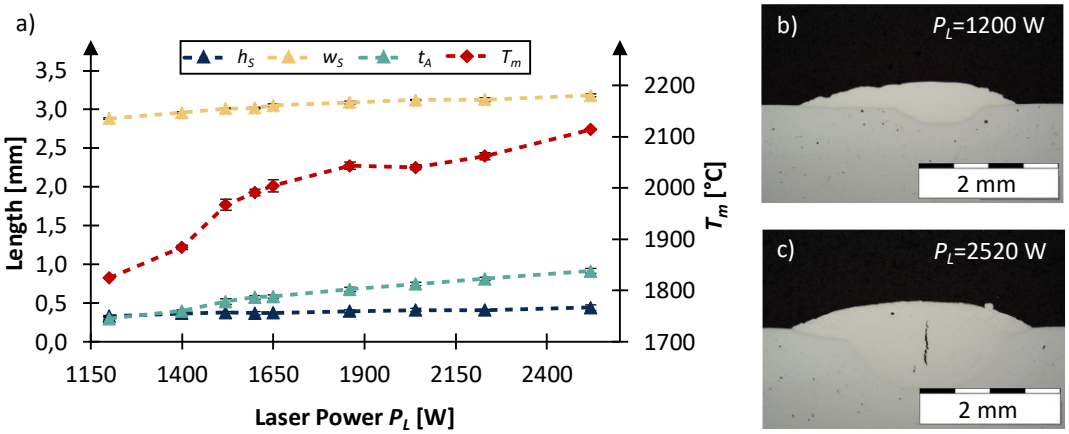

Figure 7. (a) Metallographic analysis of the parameters track height h_S, track width w_S, melt pool depth t_A and melt pool temperature T_m for different laser powers P_L; (b) cross-section of a single track with a laser power of P_L = 1200 W and (c) P_L = 2520 W

To investigate the temperature distribution within a layer and define the target melt pool temperature for the closed-loop controlled process, the first layer of the cube geometry is welded with a constant laser power of 1600 W and the cube-specific parameters. At the start of the welding process, Figure 8 shows a melt pool temperature of 2014 °C in the beginning. With an average increase of 4.1 °C/s, the temperature at the end of the layer reaches 2158 °C. In consideration of process deviations, 2200 °C is defined as target temperature for the closed-loop control of the laser power.

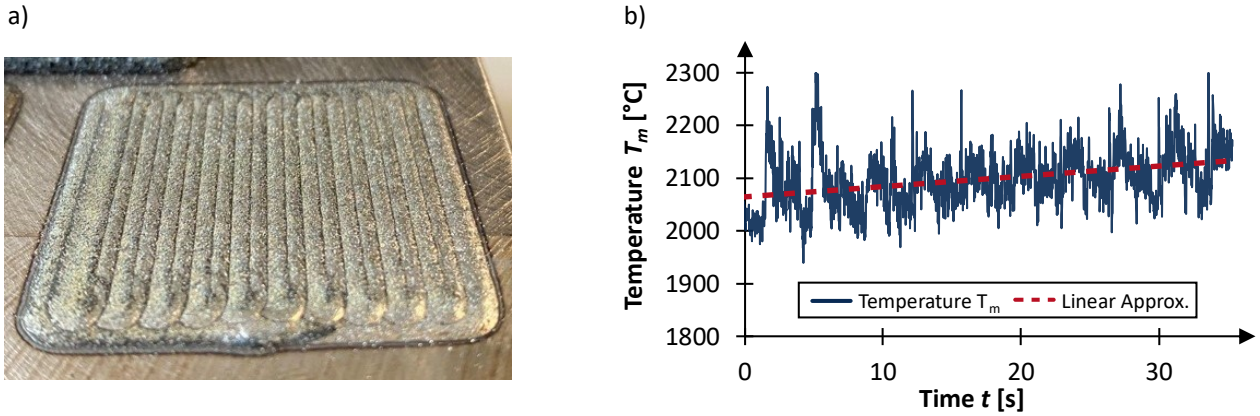

Figure 8. (a) Welding layer with a constant laser power of 1600 W and (b) related time-melt pool temperature data

Previous experiments demonstrate a suitable parameter set for a welding process with a defect-free bonding zone. In the next step, the closed-loop control is used for the additive build-up of a cube geometry. The results are compared with a cube manufactured with constant laser power. Figure 9 illustrates the geometries of both cubes after the welding process and a comparison to the ideal CAD model. For a constant laser power of 1600 W, Figures 9 a) and c) show that an insufficient part height is measured at the edges of the cube, while an oversize build-up of 0.62 mm is reached in the centre of the part. The results of the cube welded with a closed-loop control in Figure 9 b) and d) show a more even surface with lower geometric deviations of up to 1.1 mm. However, the geometric accuracy is also impaired by an 0.75 mm underbuilding of the part in the centre of the component.

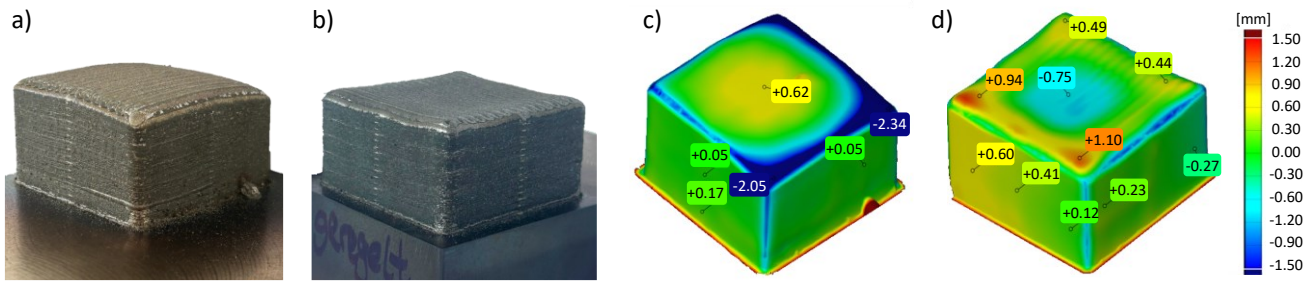

Figure 9. Validation tests with a cube geometry (a) specimen with constant laser power; (b) specimen with closed-loop control; (c) optical measurement of specimen with constant laser power; (d) optical measurement of specimen with closed-loop control

A basic requirement for the application of a tool component in the series production process of vehicle outer skin parts is a component hardness between 300 to 500 HV. To investigate the effect of the dynamically changing laser power in the closed-loop process, which can lead to different local material properties, additional hardness tests are performed for both cubes in the layers 5, 7 and 12. Figure 10 a) demonstrates that the minimum hardness of 300 HV is exceeded in all layers. For the cube welded with constant laser power, a part hardness of 335 to 342 HV is measured. In comparison, the hardness in the closed-loop process ranges between 323 to 345 HV over all measured layers of the cube. Furthermore, the etched cross sections in Figures 10 b) and c) show a uniform layer structure even at higher layers, with a decreased porosity for the closed-loop process.

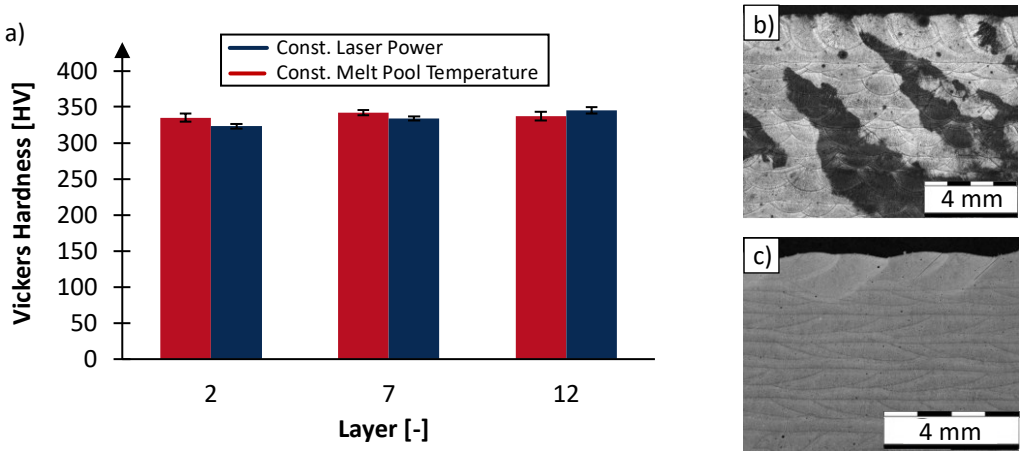

Figure 10. (a) Vickers hardness of the cube geometry with constant and closed-loop controlled laser power in the layers 2, 7 and 12; (b) cross-section of upper cube layers at constant laser power; (c) cross-section of upper cube at controlled laser power

The target geometry in this work is a shear cutting tool, which is utilized in a forming tool for the removal of excess sheet metal material to achieve the final part geometry. For the additive manufacturing process of the tool component, the developed closed-loop control is used based on the validated parameters from the previous experiment. Moreover, the CAD model of the shear cutting tool in Figure 11 a) shows that the component consists of a base body and a complex upper part. In case of a tool component repair, e.g. due to wear or crack formation, the complex part is first milled down, so the component can be rebuilt near net shape using DED. Compared to the manufacturing of a new part, this approach leads to greater material efficiency as a part milled from a solid block. The corresponding welding result is shown in Figure 11 b). While a homogeneous layer structure is obtained, the ideal component height of 25.1 mm is consistently exceeded, with a maximum height after the final layer of up to 26.9 mm. The second approach involves the manufacturing of the entire part to demonstrate the applicability of the closed-loop control for larger tool components. In this context, Figure 11 c) shows that an increasing component height does not affect the geometric accuracy. Furthermore, after the last layer of the tool component, a height between 34.8 mm and 37.4 mm is measured, which is higher than the ideal part height of 34.5 mm.

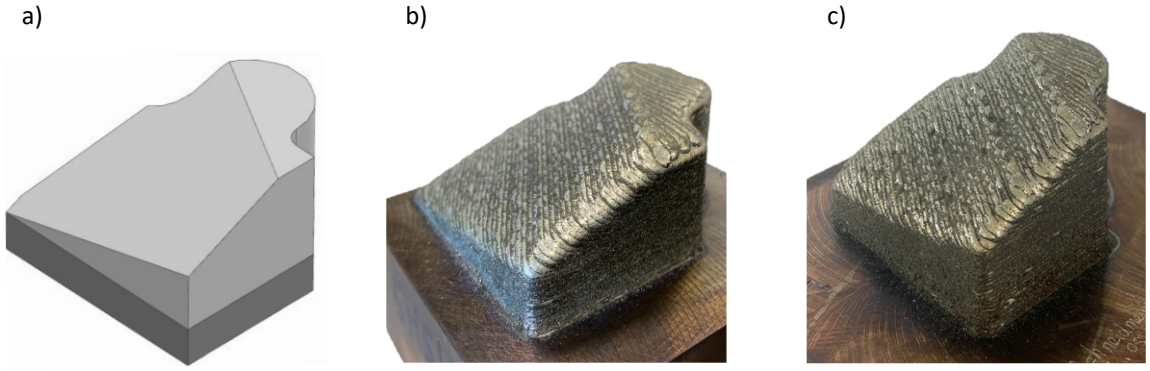

Figure 11. Tool component with base body (dark grey) and complex upper part (light grey) as (a) CAD model; (b) manufacturing result without base body; (c) manufacturing result entire geometry

4. Summary and outlook

This work investigates a melt pool temperature control for the DED-based hybrid additive manufacturing process with the objective of optimizing the geometric accuracy as well as reducing the thermal load of the part. For this reason, a substrate, consisting of the cold work steel 1.2333 with a carbon content of 0.6 %, and the powder material 3.33 LOWC were used to additively manufacture different welding geometries. The specimens were metallographically analysed and optically measured to determine geometric accuracy, mechanical properties and welding defects.

Initial investigations examined the influence of the welding parameters pyrometer spot diameter, powder mass flow, scan speed and laser power on the melt pool temperature. As the first parameter, a pyrometer spot diameter of 3.5 mm was selected, since the melt pool temperature could be measured across the entire relevant laser power range from 1520 to 2520 W. Additionally, the temperatures of the pyrometer spot diameters of 5.5 and 7.5 mm were up to 24.8 % lower, as an increasing percentage of cold areas were detected in the melt pool.

The investigation of the powder mass flow influence demonstrated that an increasing powder mass flow led to a linear reduction of the melt pool temperature by up to 10.9 %, whereby the track height increased and the meltdown depth decreased. Furthermore, to ensure a defect-free bonding zone, it was essential to use a powder mass flow above 8.5 g/min, since for lower powder mass flows vertical cracks occur in the single track due to thermal stresses.

An influence of the scan speed on the melt pool temperature became only evident at a scan speed of 25 mm/s. In contrast to a scan speed of 19 mm/s, a 4.1 % lower melt pool temperature was measured, whereby the track height was also decreased by 25.6 % as well as the melt pool depth by 14.5% due to the decreasing energy input per area.

The investigation of the laser power showed the lowest temperature deviation within a single track at constant laser power. Furthermore, an almost linear correlation between laser power and melt pool temperature was determined. While the single track height increased by up to 33.3 %, the excessive energy input of 2520 W led to crack formation inside the single track.

In this context, the metallographic analysis showed that the manufacturing parameters with a laser power of 1600 W and 2200 W, a powder mass flow of 17.9 g/min and a scan speed of 19 mm/s were suitable for the welding of a defect-free bonding zone and melt pool temperature monitoring. To define the melt pool temperature for the closed-loop controlled process of the laser power, a layer was welded in which, contrary to the single track, the temperature increased to 2158 °C by the end of the layer. Considering process deviations, a target temperature of 2200 °C was selected for further experiments. The closed-loop control was validated using a cube geometry, which was welded with constant and controlled laser power. Compared to the cube with constant laser power, where underbuilding in edge areas up to 2.34 mm was observed, the cube welded with controlled laser power showed a more even surface with a maximum negative deviation from the CAD model of 0.75 mm in the center of the cube. Furthermore, a metallographic analysis demonstrated that the required minimum hardness of 300 HV is achieved for both cubes in the layers 2,7 and 12. Finally, a tool component was manufactured using the closed-loop control of the laser power. The part height from the CAD model was constantly exceeded with an overbuilding of up to 1.8 mm for the component without base body and up to 2.6 mm for the entire tool component.

Within the scope of future investigations, the welding parameters, such as minimum laser power and waiting time between the layers, will be optimized to improve the geometric accuracy and porosity of the parts. Furthermore, the developed closed-loop control will be used for the manufacturing process of larger tool components with the aim of expanding the range of applications in toolmaking. In order to qualify the additive manufactured tool component for the series production of vehicle outer skin parts, the wear resistance will be tested in a try-out press.

References

Vasco, J. C., 2021. Additive Manufacturing for the Automotive Industry, Handbooks in Advanced Manufacturing, pp. 505-530. Available at: https://doi.or**g/**10.1016/B978-0-12-818411-0.00010-0.

Pragana, J. P. M., Sampaio, R. F. V., Bargança, I. M. F., Silva, C. M. A., Martins, P. A. F., 2021. Hybrid Metal Additive Manufacturing: A State–of–the-Art Review, Advances in Industrial and Manufacturing Engineering 2, p. 100032. Available at: https://doi.org/10.1016/j.aime.2021.100032.

Dass, A., Moridi, A., 2019. State of the Art in Directed Energy Deposition: From Additive Manufacturing to Materials Design, Coatings 9(7), p.418. Available at: https://doi.org/10.3390/coatings9070418.

Salunkhe, S., Rajamani, D., 2023. Current Trends of Metal Additive Manufacturing in the Defense, Automobile, and Aerospace Industries, Advances in Metal Additive Manufacturing, p. 147-160. Available at: https://doi.org/10.1016/B978-0-323-91230-3.00004-4.

Babuska, T. F., Krick, B. A., Susan, D. F., Kustas, A. B., 2021. Comparison of Powder Bed Fusion and Directed Energy Deposition for Tailoring Mechanical Properties of Traditionally Brittle Alloys, Manufacturing Letters 28, p. 30-34. Available at: https://doi.org/10.1016/j.mfglet.2021.02.003.

Ansari, M., Jabari, E., Toyserkani, E., 2021. Opportunities and Challenges in Additive Manufacturing of Functionally Graded Metallic Materials via Powder-Fed Laser Directed Energy Deposition: A Review, Journal of Materials Processing Technology 294, p. 117117. Available at: https://doi.org/10.1016/j.jmatprotec.2021.117117.

Feenstra, D. R., Banerjee, R., Fraser, H. L., Huang, A., Molotnikov, A., Birbilis, N., 2021. Critical Review of the State of the Art in Multi-Material Fabrication via Directed Energy Deposition, Current Opinion in Solid State & Materials Science 25(4), p. 100924. Available at: https://doi.org/10.1016/j.cossms.2021.100924.

Kumar, S., Choudhary, A. K. S., Singh, A. K., Gupta, A. K., 2016. A Comparison of Additive Manufacturing Technologies, IJIRST – International Journal for Innovative Research in Science & Technology 3(1).

Tofail, A. M., Koumoulus, E. P., Banyopadhay, A., Bose, S., O'Donoghue, L., Charidítis, C., 2018. Additive Manufacturing: Scientific and Technological Challenges, Market Uptake and Opportunities, Materials Today 21(1). Available at: https://doi.org/10.1016/j.mattod.2017.07.001.

Chechik, L., Goodall, A. D., Christofidou, K. A., Todd, I., 2023. Controlling Grain Structure in Metallic Additive Manufacturing Using a Versatile, Inexpensive Process Control System, Scientific Reports 13, p. 10003. Available at: https://doi.org/10.1038/s41598-023-37089-x.

Belitz, S., Scheider, D., Zeidler, H., 2021. Hybrid-Additive Manufacturing of Press Tools with Laser Direct Energy Deposition Using Buffer Layers to Reduce Cracking Issues, Euro PM2021 Virtual Congress & Exhibition.

Jing, H., Ge, P., Zhang, Z., Chen, J.-Q., Liu, Z.-M., Liu, W.-W., 2022. Numerical Studies of the Effects of the Substrate Structure on the Residual Stress in Laser Directed Energy Additive Manufacturing of Thin-Walled Products, Metals 12, p. 462. Available at: https://doi.org/10.3390/met12030462.

Gao, M., Wang, Z., Li, X., Zeng, X., 2013. The Effect of Deposition Patterns on the Deformation of Substrates During Direct Laser Fabrication, Journal of Engineering Materials and Technology 135(3), p. 034502. Available at: https://doi.org/10.1115/1.4024195.

Koopmann, E. T., Jäger, T. K. C., Zeidler, H., 2025. Development of Heating Strategies to Reduce Crack Formation in the Manufacturing Process of Tool Components Using Directed Energy Deposition, Progress in Additive Manufacturing 10, p. 1745-1753. Available at: https://doi.org/10.1007/s40964-025-00971-3.

Urresti, A., Murua, O., Arrizubieta, J. I., Lamikiz, A., 2024. In-Situ Monitoring of the DED-LB Process for Defect Detection, Procedia CIRP 124, p. 314-317. Available at: https://doi.org/10.1016/j.procir.2024.08.125.

Farshidianfar, M. H., Khodabakhshi, F., Khajepour, A., Gerlich, A. P., 2021. Closed-Loop Control of Microstructure and Mechanical Properties in Additive Manufacturing by Directed Energy Deposition, Materials Science & Engineering A 803, p. 140483. Available at: https://doi.org/10.1016/j.msea.2020.140483.

Maffia, S., Valentina, F., Barbara, P., 2023. Molten Pool Temperature Monitoring in Laser Metal Deposition, Mechatronics and Manufacturing 16(1), p. 96-111. Available at: https://doi.org/10.1504/IJMMS.2023.10056875.

El-Azab, S. A., Zhang, C., Jiang, S., Vyatskikh, A. L., Valdevit, L., Lavernia, E. J., Schoenung, J. M., 2023. In Situ Observation of Melt Pool Evolution in Ultrasonic Vibration Assisted Directed Energy Deposition, Scientific Reports 13, p. 17705. Available at: https://doi.org/10.1038/s41598-023-44108-4.

Ocylok, S., Alexeev, E., Mann, S., Weisheit, A., Wissenbach, K., Kelbassa, I., 2014. Correlations of Melt Pool Geometry and Process Parameters During Laser Metal Deposition by Coaxial Process Monitoring, Physics Procedia 56, p. 228 - 238. Available at: https://doi.org/10.1016/j.phpro.2014.08.167.

Ali, N., Tomesani, L., Ascari, A., Fortunato, A., 2022. Fabrication of Thin Walls with and without Close Loop Control as a Function of Scan Strategy Via Direct Energy Deposition, Lasers in Manufacturing and Materials Processing 9, p. 81-101. Available at: https://doi.org/10.1007/s40516-022-00164-8.

Song, L., Bagavath-Singh, V., Dutta, B., Mazumder, J., 2012. Control of Melt Pool Temperature and Deposition, The International Journal of Advanced Manufacturing Technology 58, p. 247-256. Available at: https://doi.org/10.1007/s00170-011-3395-2.

Bernauer, C. J., Zapataa, A., Kick, L., Tony, W., Sigl, M. E., Zaeh, M. F., 2022. Pyrometry-Based Closed-Loop Control of the Melt Pool Temperature in Laser Metal Deposition with Coaxial Wire Feeding, Procedia CIRP 111, p. 296-301. Available at: https://doi.org/10.1016/j.procir.2022.08.025.

Akbari, M., Kovacevic, R., 2019. Closed Loop Control of Melt Pool Width in Robotized Laser Powder–Directed Energy Deposition Process, The International Journal of Advanced Manufacturing Technology 104, p. 2887–2898. Available at: https://doi.org/10.1007/s00170-019-04195-y.

Smoqi, Z., Bevanas, B. D., Gaikwad, A., Craig, J., Alan, A.-H., Roeder, B., Macy, B., J. E., Prahalada, R., 2022. Closed-Loop Control of Meltpool Temperature in Directed Energy Deposition, Materials & Design 215, p. 110508. Available at: https://doi.org/10.1016/j.matdes.2022.110508.

Freeman, F., Chechich, L., Thomas, B., Todd, I., 2023. Calibrated Closed-Loop Control to Reduce the Effect of Geometry on Mechanical Behaviour in Directed Energy Deposition, Journal of Materials Processing Tech. 311, p. 117823. Available at: https://doi.org/10.1016/j.jmatprotec.2022.117823.